Hindawi
International Journal of Aerospace Engineering
Volume 2022, Article ID 8785963, 12 pages
https://doi.org/10.1155/2022/8785963

Research Article

Experimental Study on the Aerodynamic Characteristics of Blades at the Last Stage of a Steam Turbine at Off-Design Conditions

Yunfeng Liu,[1,2] **Qiankun Jia**,[1] **Xun Zhou**,[1] **Hongtao Zhang**,[2] **Yufeng Li**,[2] **Zhongqi Wang**,[1] **and Wei Du**[1]

[1]*School of Energy Science and Engineering, Harbin Institute of Technology, Harbin, China*
[2]*Harbin Turbine Company Limited, Harbin, China*

Correspondence should be addressed to Xun Zhou; zhouxun@hit.edu.cn

Received 24 July 2022; Accepted 26 August 2022; Published 9 September 2022

Academic Editor: Qingfei Fu

Experimental investigations have been carried out on the flow characteristics of the last stage long blades operating under off-design conditions. A model turbine test rig similar to a small power station was applied. The last stage blades with a scaling factor of 1 : 4.8 was used for pneumatic experiments. The rotor blade height was 375 mm, and the rotation speed was set to 7200 rpm. Five volumetric flow coefficients were utilized, corresponding to φ =0.61, 0.77, 0.92, 1.02, and 1.15. Pneumatic probes were used to focus on measuring pressures and swirl angles. The variation of different pneumatic parameters along the span and circumferential direction was investigated. The change patterns of the three-dimensional aerodynamic characteristics of the last stage blades during the off-design conditions were revealed. Results indicated that there was a high correlation between the variation of pneumatic parameters and different off-design conditions. In particular, the large meridional expansion angle at the tip led to abrupt changes in the inlet parameters, and the overlap even occupied by 17% blade height. Due to the influence of the exhaust hood, the circumferential static pressure-unevenness was up to 77.8% at the last stage outlet.

1. Introduction

The last stage long blade is the key component of the steam turbine, which has a critical impact on the power and efficiency of the generating unit [1, 2]. The last stage of the low-pressure (LP) turbine can exceed 10% of the total power of the plant, even up to 20%. Therefore, the flow characteristics at the last stage blade seriously restrict the performance of the turbine unit. To meet the challenges posed by global warming and other environmental issues, renewable energy technologies are widely used in the civil power generation field [3]. As a consequence, the large steam turbines are facing increase of peak regulation conditions [4, 5]. The peaking regulation has led to the increase in the operation of the last stage long blades under off-design conditions. It will appear separation, blockage, and other complex turbulent flow, not only endanger the blade safety but also further increase the difficulty of the last stage blade aerodynamic performance evaluation.

Part-load operation is required to pursue the thermal-economic optimization of the plant. This has resulted in a reconsideration of the aerodynamic design of today's steam turbine last stage blades, taking greater account of part-load conditions [6]. The tip/hub ratio of the last stage blades is relatively large, and the parameters are more variable along the radial direction [7]. Thus, the distinct three-dimensional flow characteristic emerges. The nozzle gradually transitions from transonic flow at the root to subsonic flow at the tip, while the rotor blade is the opposite. Bosdas et al. [8] revealed that the long rear stage blades created a relative supersonic flow field at the tip of the rotor. With the development of the advanced steam turbines, the length of

the last stage blades has been up to 1500 mm [9] and the tip/hub ratio is 2.5 [10]. The shock waves generated by the supersonic flow interact with the steam seal leakage flow near the endwall and the secondary flow [11], forming a more complex flow, as well as the non-equilibrium characteristics of wet steam [12], making it more difficult to evaluate the aerodynamic performance of the last stage blades. In addition, the damping structures such as nozzle dehumidification, rotor lacing wire, and shroud further increased the complexity of the last stage flow.

In the previous studies, numerical and experimental methods were widely applied to research the aerodynamic performance of the long last stage blades. Due to the complex and high-cost structure of the turbine test rig, a simplified structure was used in the steam turbine pneumatic experiments. Novak et al. [13] analyzed the flow field distribution of advanced 2D tip profiles of long last stage blades by experimental and numerical methods. The results indicated that due to the supersonic inlet Mach number, a vertical inlet shock wave was observed for the tip cascade. Hála et al. [14] optimized the aerodynamic design of the rotor root section within the given strength requirements. Optical and aerodynamic measurements were performed to investigate the aerodynamic characteristics of the 2D blade cascade representing the last stage rotor mid-span section including off-design conditions by Luxa et al. [15]. The results provided information on the aerodynamic characteristics of important cascades in a wide range of flow patterns including off-design conditions. Senoo and Ono [16] introduced the development of design methods for supersonic turbine airfoils and proposed methods to reduce shock wave losses. Parvizinia et al. [17] verified the aerodynamic performance of the supersonic tip section profile of a low-pressure steam turbine through numerical and experimental studies. Chaluvadi et al. [18] studied the effect of delta-wing vortex transport on the performance of the downstream blade row of a high-pressure axial-flow turbine. The above studies about the turbine blade aerodynamic characteristics only used 2D cascade profiles and air turbines, and 3D blades and wet steam turbines were not mentioned.

The steady numerical method was a reliable way to predict the aerodynamic characteristics of the low-pressure turbine's last stage during windage [19]. Liu et al. [20] and Shao et al. [21] investigated the aerodynamic characteristics of the last stage and the exhaust hood of large-scale steam turbines under different mass flow rates. It was demonstrated that high amplitude aerodynamic fluctuations were found on the rear stage rotor blades in low mass flow cases. Long last stage blades caused an increase in steam flow excitation force under off-design conditions. Cao et al. [22] investigated the parameter variation in the last stage flow field under the low flow rate cases and summarized the condensation and distribution rule of wet steam and the interaction among them. Shibukawa et al. [23] suggested that the unsteady pressure fluctuations in the turbine blade tip region probably had a high correlation with the high dynamic blade stresses through experimental studies. Hoznedl et al. [24] compared the differences in the flow fields on the left and right sides of the final stage by experiments. These differences resulted in dynamic loads on the penultimate rotor blade and potentially shortened service life. Rotor tip leakage flow and passage vortices were the main sources of unsteady flow in the last stage blades. The unsteady fluctuation of the penultimate stage increases with the increasing volumetric flow, while the rear stage decreases [25].

In this work, the three-dimensional aerodynamic performance of the steam turbine last stage blades under different off-design conditions was investigated by experimental methods. A model turbine rig was employed and the fixed and traverse pneumatic probes were used to measure pressure and velocity. The static and total pressure distributions along the span at the inlet, inter-stage, and outlet of the last stage for different volumetric flow coefficients were analyzed. The variations of the last stage reaction degree and the absolute outlet swirl angle under different flow coefficients were compared. In particular, the influence of circumferential pressure-unevenness on the aerodynamic performance of the last stage blades was considered. Eventually, this paper summarized the effects on the last stage efficiency under different off-design conditions. This work provided the fundamental insights needed to guide the design of the turbine's last stage blades.

2. Experimental Approach

2.1. Experiment Setup. Figure 1(a) presents the schematic of the rig in this study. A model steam turbine test rig is applied. This turbine test rig is similar to the rig used by Schatz and Eberle [26], which is a simplified version of a small power plant, except that the electric generator is replaced by a hydrodynamic dynamometer. The water vapor generated by the boiler flows into the high-pressure (HP) turbine and low-pressure (LP) turbine sequentially through the steam conversion valve and pipes. Meanwhile, two dynamometers are mounted on high-pressure and low-pressure turbines, respectively. The exhaust pressure is controlled by a condenser which is connected to the LP turbine. The scaling factor for the tests reported here is 1 : 4.8. And the whole off-design test is carried out in a model scale steam turbine.

As shown in Figure 1(b), the test section includes four LP turbine stages. To perform off-design tests, the three front stages and the last stage are coupled on different shafts which are called A-Rotor and B-Rotor, respectively. The HP turbine and the three front stages of the LP turbine are connected by A-Rotor, while B-Rotor is only used to drive the last stage of the LP turbine. This configuration allows not only to change B-Rotor according to different experimental requirements but also to control the speed of the last stage experimental blades individually. Moreover, the required speed is maintained by the motor dragging the experimental B-Rotor at extremely low loads, making the test section widely applicable. Besides, two dynamometers are connected to A-Rotor and B-Rotor to measure the speed and torque under different off-design conditions.

The steam turbine last stage consists of nozzles and rotor blades. According to the scaling factor, the structural parameters of the experimental blade are calculated. The parameters at the rotor blade are provided. The geometric

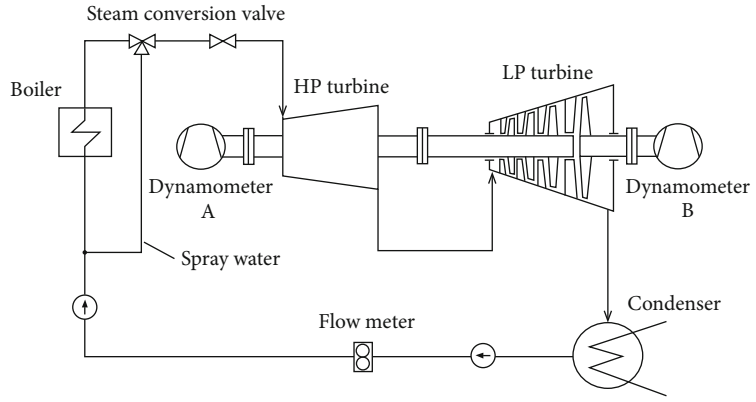

(a) Schematics of the test rig

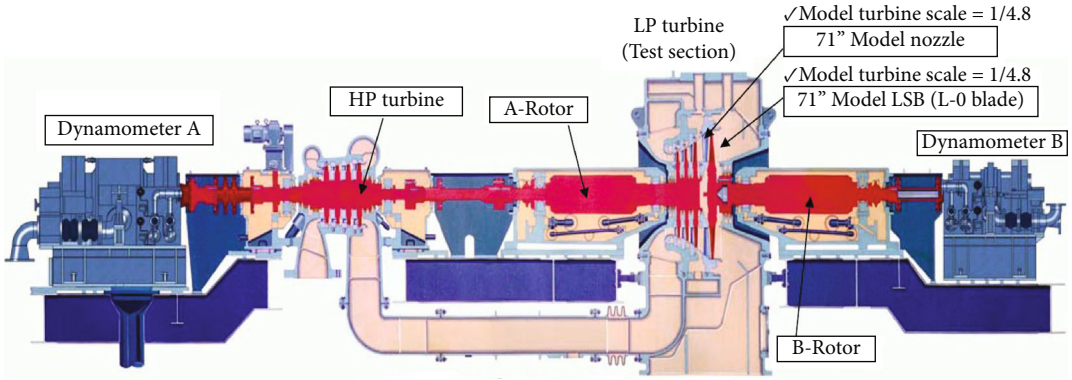

(b) Longitudinal profile of the test section

Figure 1: Model steam turbine test rig.

parameters of the experimental blades are calculated by the scaling factor. The average diameter (d) of the blade wheel and the height (h) of the rotor are 947.92 mm and 375 mm, respectively. The L-0 outlet annulus area (A_{outlet}) is 1.1167m^2 and the rotation speed (n) is set to 7200 rpm. Figure 2(a) provides some photographs of the nozzle and blade wheel, and Figure 2(b) shows the blades assembled in the model steam turbine test rig.

2.2. Pneumatic Measurement. The indication and positions of planes for measurement are shown in Figure 3. Plane 0 and plane 1 are located at the L-0 nozzle inlet and outlet, and plane 2 is positioned at the L-0 outlet. Furthermore, the effect of the non-uniform circumferential distribution of the flow on all planes is captured by circumferentially uniform arrangements of fixed and traverse probes located around the circumference. Fixed probes are used for the measurement of static pressure, while traverse probes are applied for the measurement of total pressure. Figure 3 also displays the details of the arrangement of the pneumatic probes on different measurement cross-sections. Table 1 lists the measurement parameters and probe arrangements. In particular, the velocity is measured via two five-hole probes, one located at the L-0 nozzle inlet (plane 0) and one at the L-0 outlet (plane 2).

To research the off-design aerodynamic characteristics of the last stage blades, each test has been carried out by performing volumetric flow variations whereas the exhaust pressure has been kept almost constant. Five volumetric flow coefficients are considered, φ=0.6, 0.75, 0.9, 1, and 1.1, respectively. For the model turbine test rig, the nominal volume flow (Q_{nv}) is 256.3 m^3/s, and the nominal exhaust pressure ($p_{2,nv}$) is set to 4 kPa. Actually, the measured results do not precisely match the predicted off-design conditions. To find the test conditions closest to the five predicted operating conditions, 14 operating conditions are measured during the test. Table 2 summarizes five test cases from TC1 to TC5, and the relative error of the exhaust pressure (p_2) and volumetric flow coefficients (φ) is calculated between the test value and the prediction value. The relative error of all parameters is lower than 5%. Therefore, the actual test conditions are provided, Q=0.61, 0.77, 0.92, 1.0, and 1.15 Q_{nv}. Although a slight deviation occurs, TC4 (φ=1.02) is still considered to be the design operating condition.

2.3. Parameter Definition. The volumetric flow coefficient φ is defined as [27]:

$$\varphi = \frac{Q}{Q_{nv}}, \tag{1}$$

where the volumetric flow is expressed by Q, and Q_{nv} represents the nominal volumetric flow at the design condition.

(a) L-0 nozzle and blade wheel

(b) Assembled in model steam turbine

FIGURE 2: Photos of the test rig.

Q_{nv} is calculated as:

$$Q_{nv} = A_{\text{outlet}} \cdot c_{ax}, \tag{2}$$

where A_{outlet} and c_{ax} are the L-0 stage outlet annulus area and average axial velocity.

The pressure circumferential-unevenness ξ is written as [28]:

$$\xi = \frac{p_{\max} - p_{\min}}{\bar{p}}, \tag{3}$$

where the mean static pressure is expressed by $\bar{p}$; $p_{\max}$ and $p_{\min}$ indicate the maximum and minimum static pressure.

The reaction degree Ω is defined as [29, 30]:

$$\Omega = \frac{p_1 - p_2}{p_0 - p_2}, \tag{4}$$

where p_0 and p_1 are the average static pressure for the nozzle inlet and outlet, respectively. p_2 is the average static pressure for the rotor outlet.

3. Results and Discussion

3.1. Analysis of Radial Pneumatic Parameters

3.1.1. Pressure Profile. The diameter-height ratio of the steam turbine's last stage blades is small. Therefore, the variations of the pneumatic parameters in the radial direction are highlighted. Figure 4 shows the static pressure distribution in plane 1 for different φ. It has been noticed that the static pressure distribution along the blade span of the L-0 nozzle outlet is very similar under different off-design conditions. For TC2-TC5, the static pressure increases gradually with the rise of blade span, and the max pressure appears at the tip span. The larger the flow coefficient, the higher the static pressure at the same blade span, as shown in

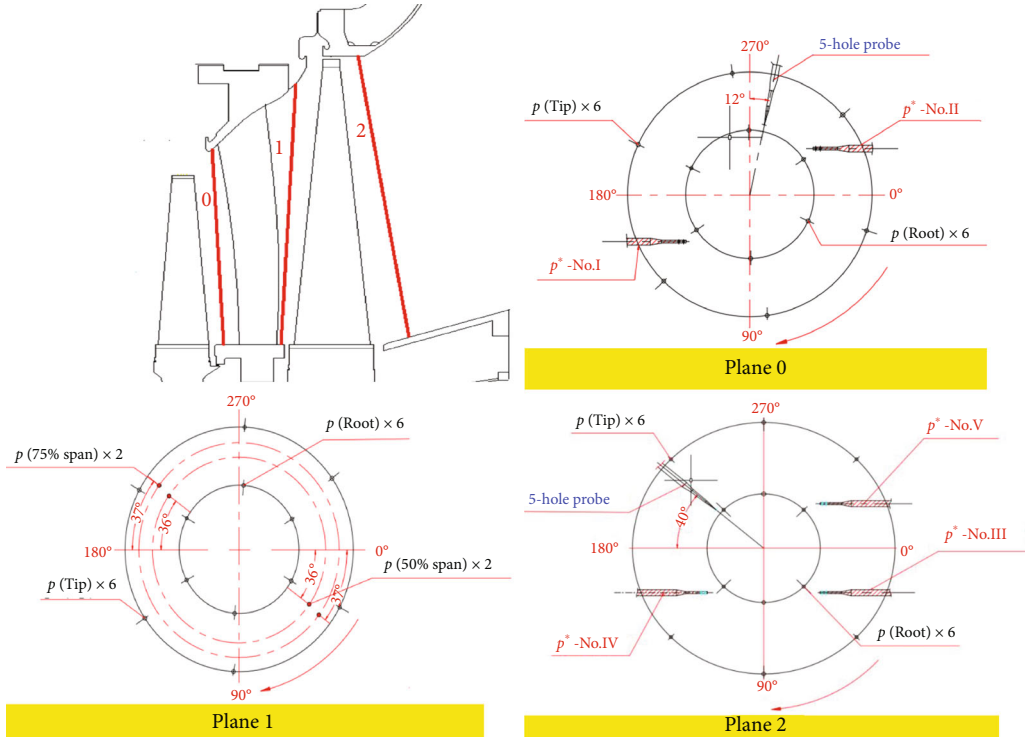

Figure 3: Indication of measurement planes and probe positions.

Table 1: Measured parameters and probe arrangements.

(a) L-0 nozzle inlet (plane 0)

Measured parameters	Probe location	Probe number	Probe type
Static pressure	Tip	6	Fixed
Static pressure	Root	6	Fixed
Total pressure	—	2	Traverse
Velocity	—	1	5-hole traverse

(b) L-0 nozzle outlet (plane 1)

Measured parameters	Probe location	Probe number	Probe type
Static pressure	Tip	6	Fixed
Static pressure	Root	6	Fixed
Static pressure	50% span	2	Fixed
Static pressure	75% span	2	Fixed

(c) L-0 outlet (plane 2)

Measured parameters	Probe location	Probe number	Probe type
Static pressure	Tip	6	Fixed
Static pressure	Root	6	Fixed
Total pressure	—	3	Traverse
Velocity	—	1	5-hole traverse

Figure 4. This demonstrates that a defined set of flow coefficients is the main driver of the pressure distribution. For all test cases, the pressure gradient presents an upward tendency at below 0.75 span. The pressure profile is relatively steep at above 0.75 span, but the pressure gradient decreases, relative to the 0.50-0.75 span. However, the static pressure is reduced at tip span for TC1. Therefore, the max pressure is noticed at 0.75 span for φ=0.61.

The variation of the reaction degrees at the different off-design conditions along the blade span is shown in Figure 5. It illustrates the significant growth of the Ω along the blade span from TC1 to TC5. It seems to present a similar distribution between reaction degrees and pressure. Correspondingly, the Ω is clearly reduced at the tip span for TC1 (φ =0.61). It indicates the decrease of Ω at the tip span as the φ decreases.

Figure 6 shows the total pressure distribution of the L-0 inlet and outlet at the different off-design conditions (TC2-TC5). In the studied test cases, an identical trend is obvious. It is demonstrated that the inlet total pressure highly depends on the changes of flow coefficient. Although the total pressure is essentially constant from the bottom to the tip, two distinct pressure pulsations are noticed at 0.55 span and tip span, as shown in Figure 6(a). It is possible that the inlet total pressure is affected by the penultimate stage rotor lacing wire at the 0.55 span. In addition, the tip overlap of the penultimate rotor blade and the rear stage nozzle accounts for 17% of the rear stage nozzle inlet, and the height is 46 mm by measurement. Due to the influence of tip leakage flow of the penultimate stage rotor blade and the diaphragm cavity, there is a significant drop in the total

Table 2: Summary of test cases.

Test condition	Exhaust pressure (p_2) [kPa]			φ		
	Test	Prediction	Relative error (%)	Test	Prediction	Relative error (%)
TC1	3.80	4	5	0.61	0.60	1.67
TC2	4.16	4	4	0.77	0.75	2.67
TC3	3.98	4	0.5	0.92	0.90	2.22
TC4	4.06	4	1.5	1.02	1.00	2
TC5	4.13	4	3.25	1.15	1.10	4.55

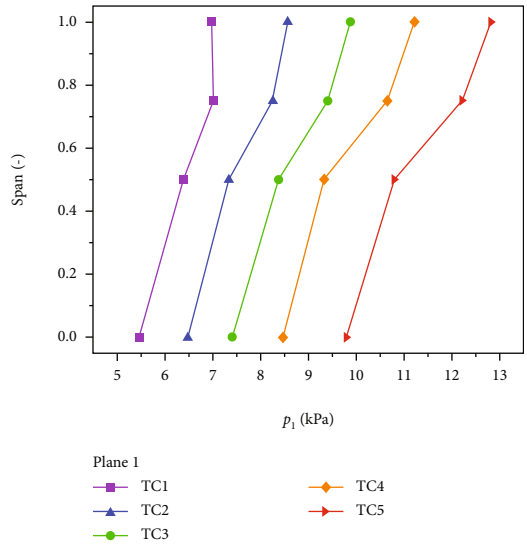

Figure 4: Static pressure distribution in plane 1 for different φ.

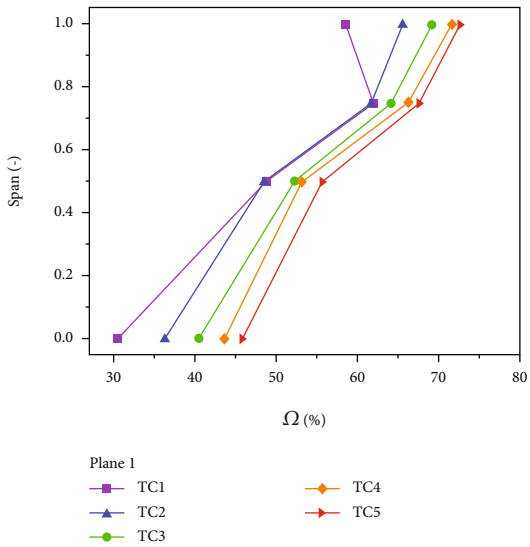

Figure 5: Reaction degree distribution for different φ.

pressure, which indicates that the loss increases in the blade tip region. Figure 6(b) depicts the distribution of total pressure in the L-0 outlet. It presents that the outlet total pressure gradually decreases along the span. For TC3, TC4, and TC5, the φ is the main driver of the total pressure variation at the same span. The pressure pulsations are also observed at the 0.4 span and tip span in all studied cases. However, the total pressure increases firstly and then decreases at the tip span, which is the opposite of the result in Figure 6(a). In particular, for the off-design conditions (TC4 and TC5) with high φ, pressure pulsation also appears at the bottom span, which is not observed in TC2 and TC3. In addition, the results show that the measured pressure difference between TC2 and TC3 is less than 0.5 kPa.

3.1.2. Swirl Angle Profile. The swirl angle is defined as the angle between the absolute velocity and the axial direction. Actually, the swirl angle is considered the key parameter to reflect the performance of the steam turbine last stage blades, especially the outlet absolute swirl angle, which has a great influence on the Leaving Loss. The α_0 and α_2 along the blade span for all test cases are displayed in Figure 7, respectively. It is easy to find the variations of the inlet and outlet swirl angles at the different φ, and also the total pressure distribution in Figure 6. As mentioned above, high correlations between some physical quantities and the flow coefficients characterizing the stage operation are displayed. The plot of the measured inlet swirl angle profile confirms the similarity for all test cases, as shown in Figure 7(a). The α_0 gradually increases along the blade span. Due to the impact of the penultimate stage rotor lacing wire, the α_0 appears at inflection points at the 0.55 span and tip span, which is generally consistent with the total pressure profile in Figure 6(a). In Figure 7(a), the α_0 is reduced suddenly at above 0.95 span, and the larger the φ, the more the swirl angle decreases.

Figure 7(b) demonstrates that the outlet swirl angle distribution is also closely related to the off-design conditions. It is indicated that the α_2 gradually decreases with the increase of φ, which is opposite to the total pressure distribution in Figure 6(b). For almost all test cases, the α_2 follows the same tendency along the span, except for the TC1 (φ =0.61). Compared with Figure 6(b), the outlet swirl angle pulsation at 0.4 span from TC2 to TC5 is also demonstrated. However, near the root (less than 0.15 span), the outlet swirl angle decreases along the span, as shown in Figure 7(b). Actually, for TC1, the α_2 increases along the blade span from α_2 =10° at the root to α_2 = 50° at the tip, which indicates a strongly radial flow at the L-0 outlet. For large flow coefficients (TC3-TC5), the negative outlet swirl angles are illustrated, as shown in Figure 7(b). For TC2, the outlet swirl angle is approximately 0. This means that the outlet steam flows out of the rotor in the axial direction. The α_2 at the same off-design condition from the root to the 0.9 span is essentially constant. However, due to the tip leakage flow at the last stage rotor blade and the diaphragm cavity, the α_2 increases sharply at above 0.9 span, and the swirl angle increases by 40° in almost all studied cases (TC2-TC5).

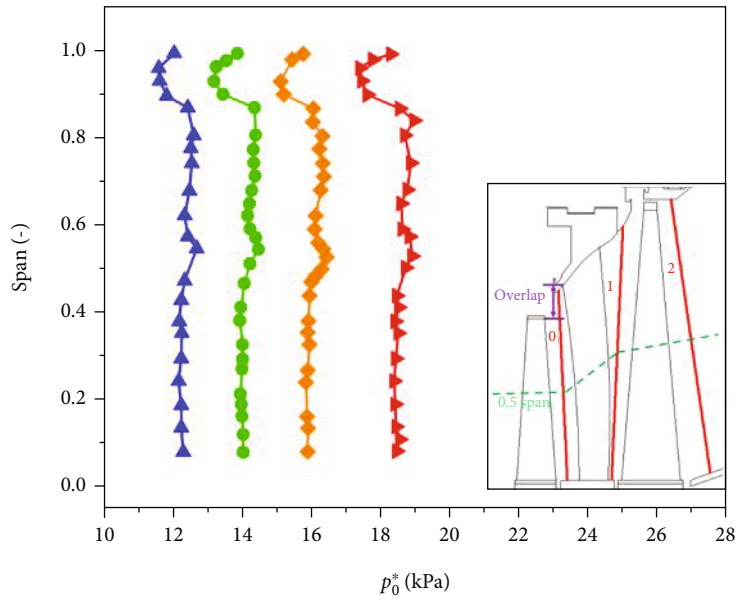

(a) Total pressure at L-0 inlet

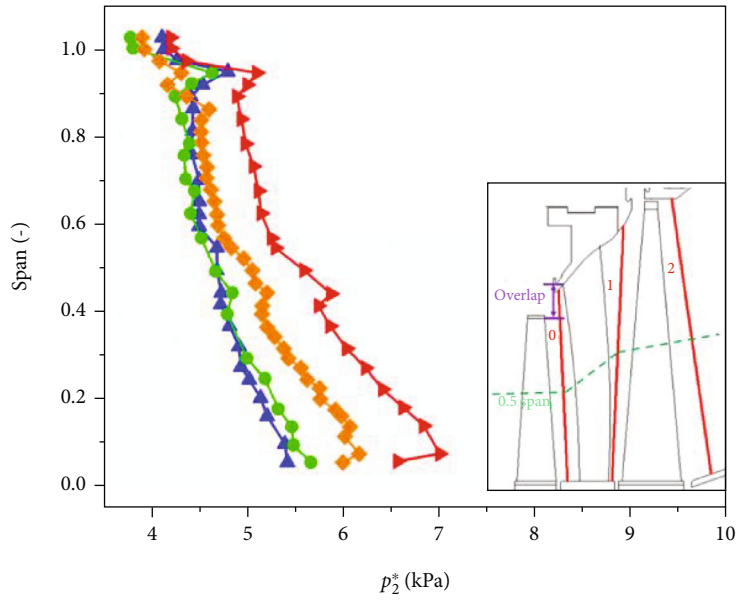

(b) Total pressure at L-0 outlet

FIGURE 6: Total pressure distribution at L-0 inlet and outlet from TC2 to TC5.

Therefore, the whole outlet swirl angle profile shows a slight C-shaped distribution.

3.2. Analysis of Circumferential Pneumatic Parameters

3.2.1. Pressure-Unevenness Study. Although the turbine final stage nozzle and rotor blades are generally symmetrically configured along the circumferential direction, the structures for extraction and exhaust are generally non-symmetrical along the circumference. The non-symmetrical arrangement structures not only cause the degradation of aerodynamic performance but even lead to uneven blade loading and bring safety problems. Figure 8 compares the variation of static pressure circumferential-

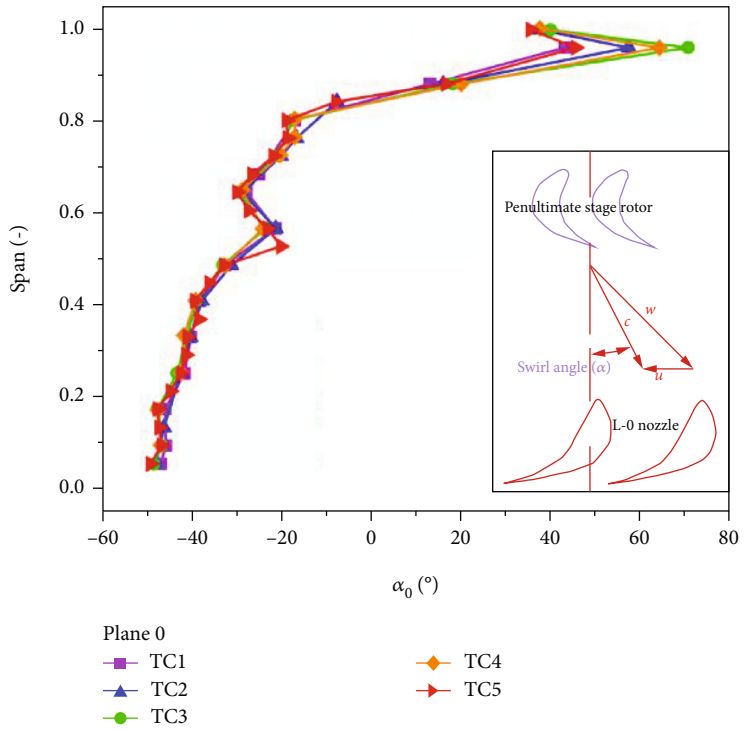

(a) Inlet swirl angle

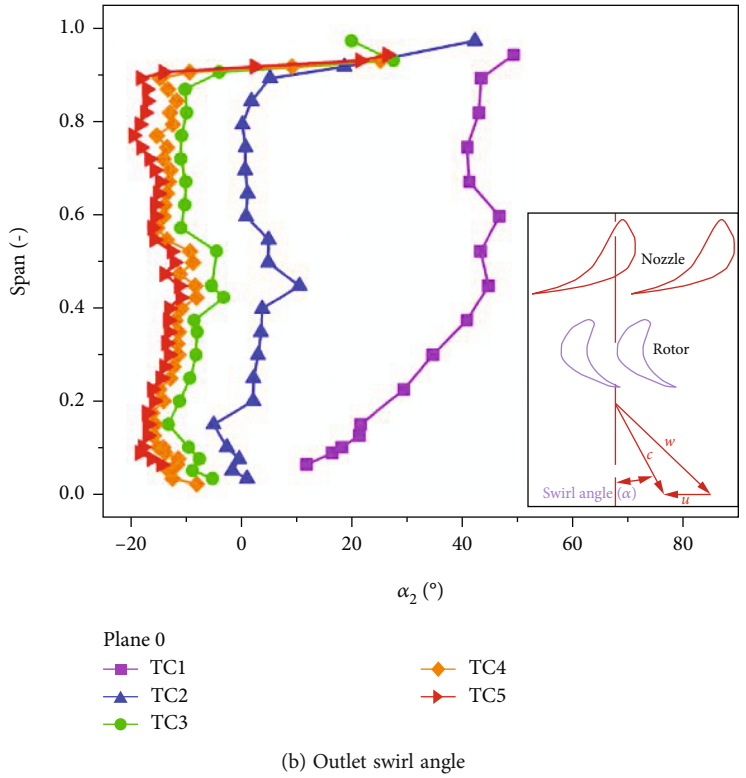

(b) Outlet swirl angle

Figure 7: Swirl angle distribution of the L-0 inlet and outlet for all test cases.

unevenness for different off-design conditions. The result indicates that the ξ at the L-0 outlet is significantly higher than that at the L-0 inlet and nozzle outlet at the different φ. In particular, the ξ at the L-0 outlet grows with the increasing flow coefficient. For the high flow coefficient cases (TC3-TC5), the ξ at the blade tip is significantly higher than at the root, and the growth rate at the tip is greater than that at the root. The measured data presents an increase of the ξ

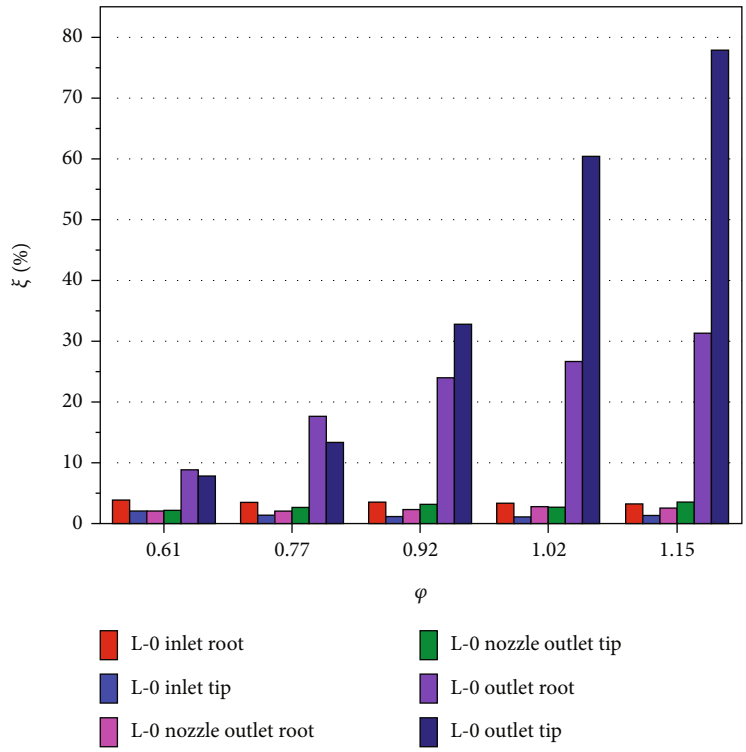

Figure 8: Comparison of static pressure circumferential-unevenness.

at the L-0 outlet root and tip by 4.7% and 17.6% from TC4 to TC5, respectively. Probably due to the effect of the rotor blade tip leakage and the diaphragm cavity, the circumferential pressure distribution at the tip presents big fluctuations in the high φ. Besides, there is the largest ξ (ξ=77.8%) at the L-0 outlet tip for TC5, as shown in Figure 8. The ξ is generally less than 5% at the L-0 inlet and nozzle outlet. It indicates that the φ is not directly relevant to the ξ of the L-0 inlet and nozzle outlet. Moreover, the ξ at the tip is distinctly lower than the root at the L-0 inlet for all test cases. However, the ξ between the tip and root remains basically at the same level at the nozzle exit. As mentioned above, the ξ displays different trends under the different off-design conditions.

3.2.2. Normalized Pressure Analysis. In Figure 9, the normalized static pressure distribution is provided to evaluate the circumferential flow non-uniformity at the root and tip of the L-0 outlet. The normalized static pressure is defined as $p/\bar{p}$. For Figure 9(a), the normalized pressure at the three measurement points (points A, B, and F) in the upper part of the outlet is higher than that in the lower part (points C, D, and E). The normalized static pressure at point A is the highest and the normalized pressure gradually increases with the increase of the φ. Meanwhile, the similar normalized pressure change strategy is shown in Figure 9(b). Most of the normalized static pressures at the points C, D, and E at the L-0 outlet root and tip are less than the average static pressure, and the higher the φ, the smaller the normalized static pressure. There is a downward exhaust facility in the model steam turbine test rig. Therefore, the closer to the bottom exhaust hood, the faster the velocity and the lower the static pressure. Compared to the root, the normalized static pressure at the tip is distinctly higher in the upper part of the L-0 outlet. However, the opposite variation is presented in the lower half. It suggests that the flow is more non-uniform at the tip, but probably more stable at the root, which is also consistent with the findings in Figure 8.

To analyze the circumferential flow non-uniformity, Figure 10 illustrates the normalized total pressure distribution at the L-0 inlet and outlet. The normalized total pressure of the inlet and outlet is defined as p^*/p_{I}^* and p^*/p_{III}^*, respectively. The arrangement of the traverse probes in plane 0 and plane 2 is illustrated in Figure 3. In Figure 10(a), the normalized total pressure is essentially uniformly distributed along the span. It confirms the flow dynamics similarity among TC1, TC3, and TC5 at the L-0 inlet. In addition, the normalized total pressure fluctuation appears at the tip span. Due to the effect of the penultimate stage tip overlap, it may lead to uneven flow across the inlet tip. As shown in Figure 9(b), the results for measurement point No. V and measurement point No. III are relatively close (the $p_{\mathrm{V}}^*/p_{\mathrm{III}}^*$ is close to 1) at the L-0 outlet. The total pressure at the measurement point 4 is relatively higher, and the $p_{\mathrm{IV}}^*/p_{\mathrm{III}}^*$ is basically between 1.05 and 1.1 at the less than 0.95 span. Probably due to the rotation direction, the rotor outlet flow deflects to the left and meets the downward flow on the left side, forming a "convergence point" that causes the local pressure (No. IV) to rise. Compared to Figure 9(b), the circumferential non-uniformity of the L-0

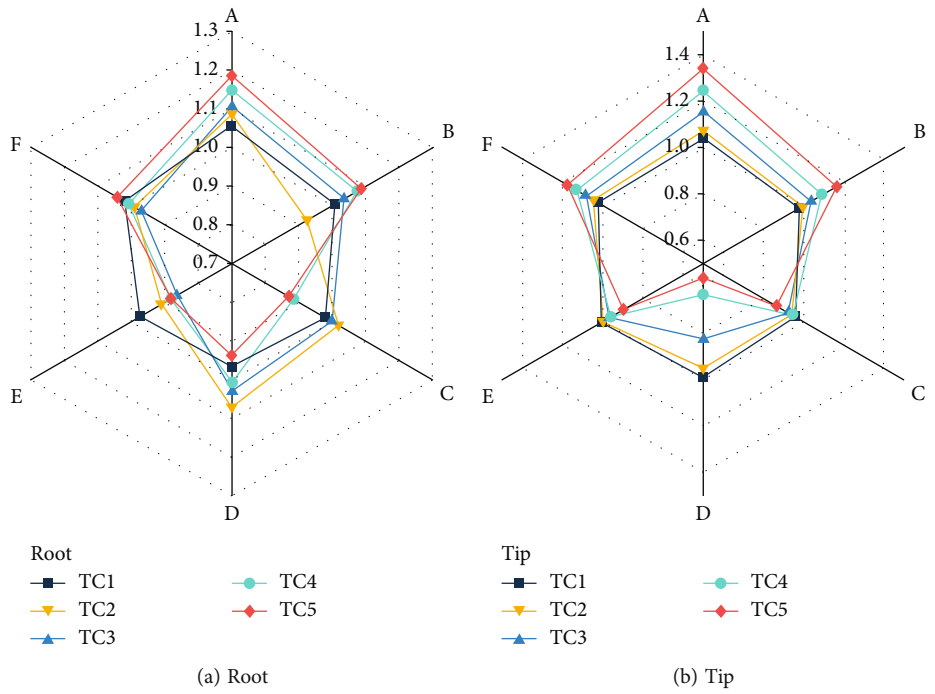

(a) Root (b) Tip

Figure 9: Normalized static pressure distribution at the L-0 outlet.

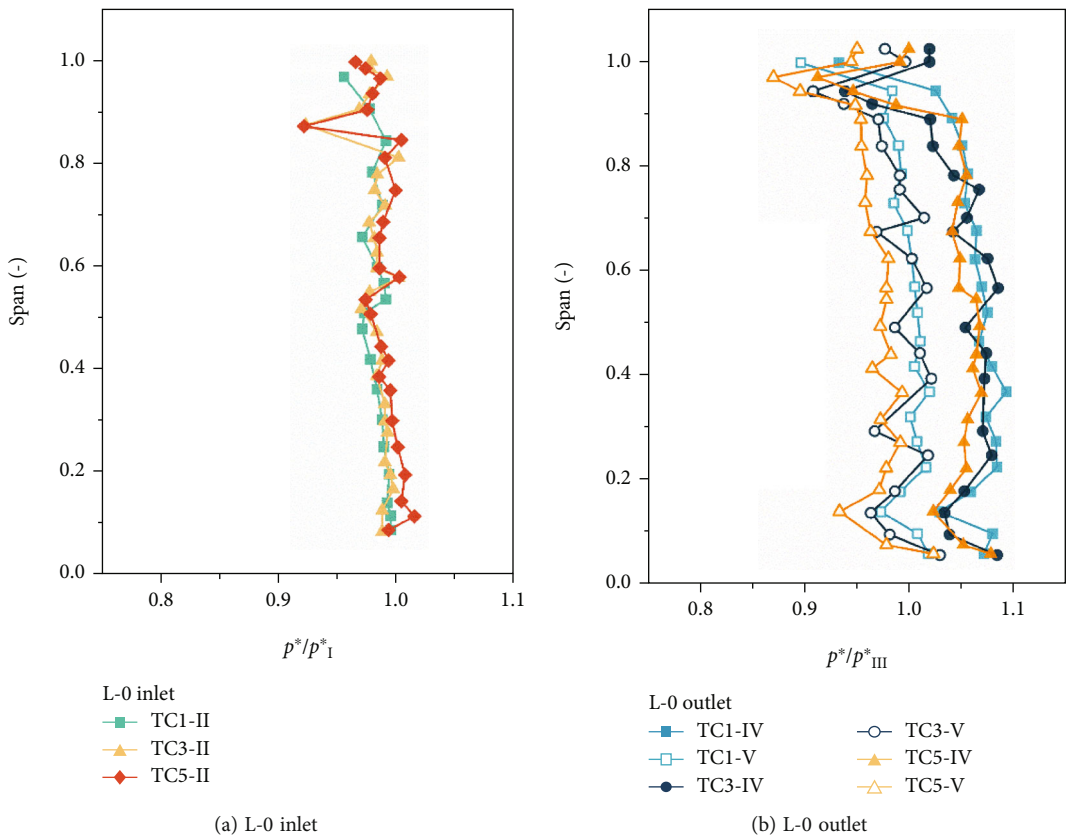

(a) L-0 inlet (b) L-0 outlet

Figure 10: Normalized total pressure distribution at the L-0 inlet and outlet.

outlet total pressure is distinctly less than the static pressure. Moreover, there is no significant correlation between the normalized total pressure distribution of the L-0 inlet and outlet and the φ.

4. Conclusions

Extensive experimental researches on the steam turbine final stage blades with five off-design conditions have been conducted. Varying the volumetric flow of the L-0 was used to characterize the off-design performance. The tests were conducted on a model steam turbine test rig with a scaling factor of 1 : 4.8. This study compared the variation of aerodynamic parameters along the radial and circumferential directions for the final stage blades with different φ. The major conclusions were summarized as follows.

(1) The off-design conditions were an essential driver of the reaction degree changes. The reaction degree gradually increases as the volumetric flow rises. For the four studied cases with the $\varphi \geq 0.77$, the reaction degree variation pattern was the same as the design condition test case (TC4). However, the reaction degree at the tip span decreased significantly for the lowest φ case (TC1). It indicated a larger shift in the three-dimensional flow, which might lead to a decrease in the final stage efficiency. Furthermore, the α_2 variation along the span was also highly correlated with different φ.

(2) The L-0 nozzle had a big meridional expansion angle, leading to a large tip overlap. Due to the influence of tip leakage flow and the diaphragm cavity, the nozzle inlet total pressure was reduced by 4% at above 0.8 span, which would lead to increased flow losses. Besides, the total pressure at the L-0 outlet decreased gradually along the span, and the effect of tip overlap was weakened

(3) The nozzle inlet circumferential flow non-uniformity was negligible, and there was no significant correlation with the off-design conditions. In addition, the flow at the L-0 outlet was non-uniform along the circumference, and the normalized static pressure was larger than the normalized total. For the five off-design conditions, the outlet total pressure non-uniformity was not clearly related to the φ, while the static pressure circumferential-unevenness increased with the increase of the φ.

(4) On the one hand, the reduction of the φ caused variations of the radial parameters, leading to a decrease in efficiency. On the other hand, the outlet circumferential non-uniformity increased with the growth of the φ, which also caused the decrease in the final stage efficiency

Nomenclature

A_{outlet}: Outlet annulus area
d: Blade wheel average diameter [mm]
h: Blade height [mm]
HP/LP: High-pressure/low-pressure turbine
L-0: Last stage
n: Rotation speed [rpm]
p: Pressure [kPa]
Q: Volumetric flow [m^3/s]
c_{ax}: Outlet average axial velocity.

Greek symbols

α: Swirl angle [°]
Ω: Reaction degree
ξ: Static pressure circumferential-unevenness
φ: Volumetric flow coefficient.

Subscripts

0/1/2: Last stage inlet/last stage nozzle outlet/last stage outlet
$*$: Total value
nv: Nominal value
I, II, III, IV, V: Total pressure traverse probe no.

Data Availability

The data used to support the findings of this study are included within the article.

Conflicts of Interest

The authors declare that there is no conflict of interest regarding the publication of this paper.

Acknowledgments

The authors acknowledge the financial support provided by National Science and Technology Major Project (No. 2017-II-0007-0021).

References

[1] A. S. Leyzerovich, *Steam Turbines for Modern Fossil-Fuel Power Plants*, River Publishers, 2021.

[2] I. McBean, S. Havakechian, and P.-A. Masserey, "The development of long last stage steam turbine blades," *Turbo Expo: Power for Land, Sea, and Air*, vol. 7, pp. 2245–2256, 2010.

[3] International Energy Agency, *World Energy Outlook 2021*, International Energy Agency, Paris, 2021.

[4] M. Richter, F. Möllenbruck, F. Obermüller et al., "Flexibilization of steam power plants as partners for renewable energy systems," in *2016 Power Systems Computation Conference (PSCC)*, pp. 1–8, Genoa, Italy, 2016.

[5] P. Eser, A. Singh, N. Chokani, and R. S. Abhari, "Effect of increased renewables generation on operation of thermal power plants," *Applied Energy*, vol. 164, pp. 723–732, 2016.

[6] A. S. Karakurt, "Performance analysis of a steam turbine power plant at part load conditions," *Journal of Thermal Engineering*, vol. 3, no. 2, pp. 1121–1128, 2017.

[7] T. Tanuma, "Development of last-stage long blades for steam turbines," in *Advances in Steam Turbines for Modern Power Plants, Woodhead Publishing*, pp. 279–305, Woodhead Publishing, 2017.

[8] I. Bosdas, M. Mansour, A. I. Kalfas, R. S. Abhari, and S. Senoo, "Unsteady flow field and coarse droplet measurements in the

last stage of a low-pressure steam turbine with supersonic airfoils near the blade tip," *Journal of Engineering for Gas Turbines and Power*, vol. 139, no. 9, 2017.

[9] H. Fukuda, H. Ohyama, T. Miyawaki, K. Mori, Y. Kadoya, and Y. Hirakawa, "Development of 3,600-rpm 50-inch/3,000-rpm 60-inch ultra-long exhaust end blades," *Mitsubishi Heavy Industries Technical Review*, vol. 46, no. 2, pp. 18–25, 2009.

[10] S. Senoo, H. Ono, T. Shibata et al., "Development of titanium 3600rpm-50inch and 3000rpm-60inch last stage blades for steam turbines," *International Journal of Gas Turbine, Propulsion and Power Systems*, vol. 6, no. 2, pp. 9–16, 2014.

[11] C. Liu, J. Zhang, D. Jia, and P. Li, "Experimental and numerical investigation of the transition progress of strut-induced wakes in the supersonic flows," *Aerospace Science and Technology*, vol. 120, p. 107256, 2022.

[12] L. Li, Y. Li, X. Xie, and J. Li, "Quantitative evaluation of wetness losses in steam turbines based on three-dimensional simulations of non-equilibrium condensing flows," *Proceedings of the Institution of Mechanical Engineers, Part A: Journal of Power and Energy*, vol. 228, no. 6, pp. 708–716, 2014.

[13] O. Novak, M. Bobcik, M. Luxa et al., "Turbine cascades of last stage blades for wide range of operating conditions," *International Journal of Turbomachinery, Propulsion and Power*, vol. 4, no. 4, p. 33, 2019.

[14] J. Hála, M. Luxa, D. Šimurda et al., "Optimization of root section for ultra-long steam turbine rotor blade," *Journal of Thermal Science*, vol. 27, no. 2, pp. 95–102, 2018.

[15] M. Luxa, D. Šimurda, P. Safarik, J. Synác, and B. Rudas, "High-speed aerodynamic investigation of the midsection of a 48 rotor blade for the last stage of steam turbine," in *10th European Conference on Turbomachinery Fluid Dynamics & Thermodynamics*, Lappeenranta, 2013.

[16] S. Senoo and H. Ono, "Development of design method for supersonic turbine aerofoils near the tip of long blades in steam turbines: part 2—configuration details and validation," *Turbo Expo: Power for Land, Sea, and Air*, vol. 55201, article V05BT25A002, 2013.

[17] M. Parvizinia, C. Berlich, F. Truckenmüller, and H. Stuër, "Numerical and experimental investigations into the aerodynamic performance of a supersonic turbine blade profile," *Turbo Expo: Power for Land, Sea, and Air*, vol. 41707, pp. 1349–1358, 2004.

[18] V. Chaluvadi, A. Kalfas, and H. Hodson, "Vortex transport and blade interactions in high pressure turbines," *Journal of Turbomachinery*, vol. 126, no. 3, pp. 395–405, 2004.

[19] R. Sigg, C. Heinz, M. Casey, and N. Sürken, "Numerical and experimental investigation of a low-pressure steam turbine during windage," *Proceedings of the Institution of Mechanical Engineers, Part A: Journal of Power and Energy*, vol. 223, no. 6, pp. 697–708, 2009.

[20] B. Liu, J. Yang, D. Zhou, X. Zhu, and Z. Du, "Numerical investigations of flow features in a low pressure steam turbine last stage under different mass flow rates," *Turbo Expo: Power for Land, Sea, and Air*, vol. 56796, article V008T26A022, 2015.

[21] S. Shao, Q. Deng, H. Shi, Z. Feng, K. Cheng, and Z. Peng, "Numerical investigation on flow characteristics of low pressure exhaust hood under off-design conditions for steam turbines," *Turbo Expo: Power for Land, Sea, and Air*, vol. 5B, article V05BT25A031, 2013.

[22] L. Cao, J. Wang, H. Luo, H. Si, and R. Yang, "Distribution of condensation droplets in the last stage of steam turbine under small flow rate condition," *Applied Thermal Engineering*, vol. 181, p. 116021, 2020.

[23] N. Shibukawa, T. Tejima, Y. Iwasaki, I. Murakami, and I. Saito, "A correlation between vibration stresses and flow features of steam turbine long blades in low load conditions," *Turbo Expo: Power for Land, Sea, and Air*, vol. 7, pp. 2437–2446, 2011.

[24] M. Hoznedl, M. Kolovratník, O. Bartoš, K. Sedlák, R. Kalista, and L. Mrózek, "Experimental research on the flow at the last stage of a 1090 MW steam turbine," *Proceedings of the Institution of Mechanical Engineers, Part A: Journal of Power and Energy*, vol. 232, no. 5, pp. 515–524, 2018.

[25] I. Bosdas, M. Mansour, A. I. Kalfas, R. S. Abhari, and S. Senoo, "Unsteady wet steam flow field measurements in the last stage of low pressure steam turbine," *Journal of Engineering for Gas Turbines and Power*, vol. 138, no. 3, 2016.

[26] M. Schatz and T. Eberle, "Experimental study of steam wetness in a model steam turbine rig: presentation of results and comparison with computational fluid dynamics data," *Proceedings of the Institution of Mechanical Engineers, Part A: Journal of Power and Energy*, vol. 228, no. 2, pp. 129–142, 2014.

[27] A. Mambro, F. Congiu, E. Galloni, and L. Canale, "Experimental study and modelling of the ventilation power and maximum temperature of low-pressure steam turbine last stages at low load," *Applied Energy*, vol. 241, pp. 59–72, 2019.

[28] J. Gao, M. Wei, W. Fu, Q. Zheng, and G. Yue, "Experimental and numerical investigations of trailing edge injection in a transonic turbine cascade," *Aerospace Science and Technology*, vol. 92, pp. 258–268, 2019.

[29] S. L. Dixon and C. Hall, *Fluid Mechanics and Thermodynamics of Turbomachinery*, Butterworth-Heinemann, 2013.

[30] W. Gardner, *Energy Efficient Engine: High Pressure Turbine Uncooled Rig Technology Report*, 1979.